CLNS 99/1652
CLEO 99-19

Study of Charmless Hadronic B Meson Decays to Pseudoscalar-Vector Final States

CLEO Collaboration

(June 1, 2000)

Abstract

We report results of searches for charmless hadronic B meson decays to pseudoscalar($\pi^{\pm}$, $K^{\pm}$, π^0 or K_S^0)-vector(ρ, K^* or ω) final states. Using 9.7×10^6 $B\bar{B}$ pairs collected with the CLEO detector, we report first observation of $B^- \to \pi^-\rho^0$, $\bar{B}^0 \to \pi^{\pm}\rho^{\mp}$ and $B^- \to \pi^-\omega$, which are expected to be dominated by hadronic $b \to u$ transitions. The measured branching fractions are $(10.4^{+3.3}_{-3.4} \pm 2.1) \times 10^{-6}$, $(27.6^{+8.4}_{-7.4} \pm 4.2) \times 10^{-6}$ and $(11.3^{+3.3}_{-2.9} \pm 1.4) \times 10^{-6}$, respectively. Branching fraction upper limits are set for all the other decay modes investigated.

PACS numbers: 13.20.He,13.25.-k,13.25.Hw,13.30.Eg,14.40.Nd

C. P. Jessop,[1] H. Marsiske,[1] M. L. Perl,[1] V. Savinov,[1] D. Ugolini,[1] X. Zhou,[1] T. E. Coan,[2] V. Fadeyev,[2] Y. Maravin,[2] I. Narsky,[2] R. Stroynowski,[2] J. Ye,[2] T. Wlodek,[2] M. Artuso,[3] R. Ayad,[3] C. Boulahouache,[3] K. Bukin,[3] E. Dambasuren,[3] S. Karamov,[3] G. Majumder,[3] G. C. Moneti,[3] R. Mountain,[3] S. Schuh,[3] T. Skwarnicki,[3] S. Stone,[3] G. Viehhauser,[3] J.C. Wang,[3] A. Wolf,[3] J. Wu,[3] S. Kopp,[4] S. E. Csorna,[5] I. Danko,[5] K. W. McLean,[5] Sz. Márka,[5] Z. Xu,[5] R. Godang,[6] K. Kinoshita,[6,*] I. C. Lai,[6] S. Schrenk,[6] G. Bonvicini,[7] D. Cinabro,[7] S. McGee,[7] L. P. Perera,[7] G. J. Zhou,[7] E. Lipeles,[8] M. Schmidtler,[8] A. Shapiro,[8] W. M. Sun,[8] A. J. Weinstein,[8] F. Würthwein,[8,†] D. E. Jaffe,[9] G. Masek,[9] H. P. Paar,[9] E. M. Potter,[9] S. Prell,[9] V. Sharma,[9] D. M. Asner,[10] A. Eppich,[10] T. S. Hill,[10] R. J. Morrison,[10] H. N. Nelson,[10] R. A. Briere,[11] B. H. Behrens,[12] W. T. Ford,[12] A. Gritsan,[12] J. Roy,[12] J. G. Smith,[12] J. P. Alexander,[13] R. Baker,[13] C. Bebek,[13] B. E. Berger,[13] K. Berkelman,[13] F. Blanc,[13] V. Boisvert,[13] D. G. Cassel,[13] M. Dickson,[13] P. S. Drell,[13] K. M. Ecklund,[13] R. Ehrlich,[13] A. D. Foland,[13] P. Gaidarev,[13] L. Gibbons,[13] B. Gittelman,[13] S. W. Gray,[13] D. L. Hartill,[13] B. K. Heltsley,[13] P. I. Hopman,[13] C. D. Jones,[13] D. L. Kreinick,[13] M. Lohner,[13] A. Magerkurth,[13] T. O. Meyer,[13] N. B. Mistry,[13] E. Nordberg,[13] J. R. Patterson,[13] D. Peterson,[13] D. Riley,[13] J. G. Thayer,[13] P. G. Thies,[13] B. Valant-Spaight,[13] A. Warburton,[13] P. Avery,[14] C. Prescott,[14] A. I. Rubiera,[14] J. Yelton,[14] J. Zheng,[14] G. Brandenburg,[15] A. Ershov,[15] Y. S. Gao,[15] D. Y.-J. Kim,[15] R. Wilson,[15] T. E. Browder,[16] Y. Li,[16] J. L. Rodriguez,[16] H. Yamamoto,[16] T. Bergfeld,[17] B. I. Eisenstein,[17] J. Ernst,[17] G. E. Gladding,[17] G. D. Gollin,[17] R. M. Hans,[17] E. Johnson,[17] I. Karliner,[17] M. A. Marsh,[17] M. Palmer,[17] C. Plager,[17] C. Sedlack,[17] M. Selen,[17] J. J. Thaler,[17] J. Williams,[17] K. W. Edwards,[18] R. Janicek,[19] P. M. Patel,[19] A. J. Sadoff,[20] R. Ammar,[21] A. Bean,[21] D. Besson,[21] R. Davis,[21] N. Kwak,[21] X. Zhao,[21] S. Anderson,[22] V. V. Frolov,[22] Y. Kubota,[22] S. J. Lee,[22] R. Mahapatra,[22] J. J. O'Neill,[22] R. Poling,[22] T. Riehle,[22] A. Smith,[22] J. Urheim,[22] S. Ahmed,[23] M. S. Alam,[23] S. B. Athar,[23] L. Jian,[23] L. Ling,[23] A. H. Mahmood,[23,‡] M. Saleem,[23] S. Timm,[23] F. Wappler,[23] A. Anastassov,[24] J. E. Duboscq,[24] K. K. Gan,[24] C. Gwon,[24] T. Hart,[24] K. Honscheid,[24] D. Hufnagel,[24] H. Kagan,[24] R. Kass,[24] T. K. Pedlar,[24] H. Schwarthoff,[24] J. B. Thayer,[24] E. von Toerne,[24] M. M. Zoeller,[24] S. J. Richichi,[25] H. Severini,[25] P. Skubic,[25] A. Undrus,[25] S. Chen,[26] J. Fast,[26] J. W. Hinson,[26] J. Lee,[26] N. Menon,[26] D. H. Miller,[26] E. I. Shibata,[26] I. P. J. Shipsey,[26] V. Pavlunin,[26] D. Cronin-Hennessy,[27] Y. Kwon,[27,§] A.L. Lyon,[27] and E. H. Thorndike[27]

[1]Stanford Linear Accelerator Center, Stanford University, Stanford, California 94309
[2]Southern Methodist University, Dallas, Texas 75275
[3]Syracuse University, Syracuse, New York 13244
[4]University of Texas, Austin, TX 78712

---

[*]Permanent address: University of Cincinnati, Cincinnati, OH 45221

[†]Permanent address: Massachusetts Institute of Technology, Cambridge, M A 02139.

[‡]Permanent address: University of Texas - Pan American, Edinburg, TX 78 539.

[§]Permanent address: Yonsei University, Seoul 120-749, Korea.

[5]Vanderbilt University, Nashville, Tennessee 37235
[6]Virginia Polytechnic Institute and State University, Blacksburg, Virginia 24061
[7]Wayne State University, Detroit, Michigan 48202
[8]California Institute of Technology, Pasadena, California 91125
[9]University of California, San Diego, La Jolla, California 92093
[10]University of California, Santa Barbara, California 93106
[11]Carnegie Mellon University, Pittsburgh, Pennsylvania 15213
[12]University of Colorado, Boulder, Colorado 80309-0390
[13]Cornell University, Ithaca, New York 14853
[14]University of Florida, Gainesville, Florida 32611
[15]Harvard University, Cambridge, Massachusetts 02138
[16]University of Hawaii at Manoa, Honolulu, Hawaii 96822
[17]University of Illinois, Urbana-Champaign, Illinois 61801
[18]Carleton University, Ottawa, Ontario, Canada K1S 5B6
and the Institute of Particle Physics, Canada
[19]McGill University, Montréal, Québec, Canada H3A 2T8
and the Institute of Particle Physics, Canada
[20]Ithaca College, Ithaca, New York 14850
[21]University of Kansas, Lawrence, Kansas 66045
[22]University of Minnesota, Minneapolis, Minnesota 55455
[23]State University of New York at Albany, Albany, New York 12222
[24]Ohio State University, Columbus, Ohio 43210
[25]University of Oklahoma, Norman, Oklahoma 73019
[26]Purdue University, West Lafayette, Indiana 47907
[27]University of Rochester, Rochester, New York 14627

CP violation in the Standard Model (SM) is a consequence of the complex phase in the Cabibbo-Kobayashi-Maskawa (CKM) quark-mixing matrix [1]. The study of charmless hadronic decays of B mesons plays a key role in testing the SM picture of CP violation. For example, the angle $\alpha \equiv arg$ $[(-V_{td}V_{tb}^*)/(V_{ud}V_{ub}^*)]$ of the unitarity triangle can be measured by performing a full Dalitz analysis of the decays $B^0(\bar{B}^0) \to \pi^+\rho^-$, $\pi^-\rho^+$ and $\pi^0\rho^0$ [2]. While the CLEO data do not yet have the sensitivity for the CP violation measurements, experimental measurements of these decay modes will be useful to test various theoretical predictions that typically make use of effective Hamiltonians, often with factorization assumptions [3]. Recently, it has been suggested [4] that published experimental results on charmless hadronic B decays indicate that $\cos\gamma < 0$, in disagreement with current fits to the information most sensitive to CKM matrix elements [5].

In this Letter, we present results of searches for B meson decays to exclusive pseudoscalar-vector ($B \to PV$) final states that include a pseudoscalar meson $\pi^\pm$, $K^\pm$, π^0 or K_S^0 and a vector meson ρ, K^* or ω. In particular we present first observation of the decays $B^- \to \pi^-\rho^0$, $\bar{B}^0 \to \pi^\pm\rho^\mp$ and $B^- \to \pi^-\omega$ (charge-conjugate modes are implied) which are expected to be dominated by hadronic $b \to u$ transitions. Our results supersede previous CLEO results on these decay modes [6].

The data were collected with two configurations (CLEO II [7] and CLEO II.V [8]) of the CLEO detector at the Cornell Electron Storage Ring (CESR). They consist of 9.1 fb^{-1} taken at the Υ(4S), which corresponds to 9.7×10^6 $B\bar{B}$ pairs, and 4.4 fb^{-1} taken below $B\overline{B}$ threshold, used for continuum background studies. The data sample contains a factor of 3 more statistics than previously published results [6]. In addition, the CLEO II data were reanalyzed with improved calibration and track-fitting, allowing for larger geometric acceptance and more efficient track quality requirements.

The final states of the decays under study are reconstructed by combining detected photons and charged pions and kaons. The detector elements most important for the results presented here are the tracking system, which consists of several concentric detectors operating inside a 1.5 T superconducting solenoid, and the high-resolution electromagnetic calorimeter, consisting of 7800 CsI(Tl) crystals. For CLEO II, the tracking system consists of a 6-layer straw tube chamber, a 10-layer precision drift chamber, and a 51-layer main drift chamber. The main drift chamber also provides a measurement of the specific ionization loss, dE/dx, used for particle identification. For CLEO II.V the straw tube chamber was replaced by a 3-layer, double-sided silicon vertex detector, and the gas in the main drift chamber was changed from an argon-ethane to a helium-propane mixture.

The resonances in the final state are identified via the decay modes $\rho \to \pi\pi$, $K^* \to K\pi$ ($K^{*0} \to K^+\pi^-$, $K^{*+} \to K^+\pi^0$) and $\omega \to \pi^+\pi^-\pi^0$. Reconstructed charged tracks are required to pass quality cuts based on their track fit residuals and impact parameter in both the r–ϕ and r–z planes, and on the number of main drift chamber measurements. Each event must have a total of at least four such charged tracks. The dE/dx measured by the main drift chamber is used to distinguish kaons from pions. Electrons are rejected based on dE/dx information and the ratio of the measured track momentum and the associated shower energy in the calorimeter. Muons are rejected by requiring that charged tracks penetrate fewer than seven interaction lengths of material. Pairs of charged tracks used to reconstruct K_S^0 (via $K_S^0 \to \pi^+\pi^-$) are required to have a common vertex displaced from the primary interaction point. The invariant mass of the two charged pions is required to be within two standard deviations (σ) of the known K_S^0 mass [9]. Furthermore, the K_S^0 momentum vector, obtained from a kinematic fit of the charged pions' momenta, is required to point back to the beam spot. To form π^0 candidates, pairs of photon candidates with an invariant mass within 2.5σ of the nominal π^0 mass are kinematically fitted with the mass constrained to the known π^0 mass [9].

The primary means of identification of B meson candidates is through their measured mass and energy. The beam-constrained mass of the candidate is defined as $M_B \equiv \sqrt{E_b^2 - |\mathbf{p}|^2}$, where $\mathbf{p}$ is the measured momentum of the candidate and E_b is the beam energy. The resolution of M_B ranges from 2.5 to 3.5 MeV, where the larger resolutions correspond to decay modes with neutral pion(s). The second observable ΔE is defined as $\Delta E \equiv E_1 + E_2 - E_b$, where E_1 and E_2 are the energies of the two final state mesons. The resolution of ΔE is mode dependent. For final states without a neutral pion, the ΔE resolution is about 20 MeV. For decay modes with one or two energetic neutral pions ($\bar{B}^0 \to \pi^\pm\rho^\mp$, $\bar{B}^0 \to \pi^0\rho^0$ and $B^- \to \pi^0\rho^-$ etc), the ΔE resolution worsens by approximately a factor of 2 or 3 and becomes slightly asymmetric because of energy loss out of the back of the CsI crystals. We accept events with $M_B > 5.2$ GeV and $|\Delta E| < 100$ to 300 MeV depending on the decay mode.

The vector meson ρ, K^* and ω candidates are required to have masses within 200, 75 and 50 MeV of their known masses [9], respectively. In the simultaneous analysis of $\bar{B}^0 \to \pi^0\rho^0$ and $\pi^0 K^{*0}$, the ρ^0 or K^{*0} candidate is required to have mass between 0.3 GeV to 1.0 GeV under the $\pi^+\pi^-$ decay hypothesis so that both ρ^0 and K^{*0} enter into the sample. Because of the polarization of the vector meson, the soft decay product from the vector meson may have momentum as low as 150 MeV. To reduce the large combinatoric background from soft π^0s, only half of the helicity ($\mathcal{H}$) range, corresponding to a hard π^0, is selected when a ρ^+ or K^{*+} decays to a $\pi^+\pi^0$ or $K^+\pi^0$. The helicity is defined as the cosine of the angle between one of the vector meson decay products in the vector meson rest frame and the direction of the vector meson momentum in the lab frame.

The main background comes from continuum $e^+e^- \to q\bar{q}$, where $q = u$, d, s, c. This background typically exhibits a two-jet structure and can be reduced with event shape criteria. We calculate the angle θ_S (θ_T) between the sphericity axis [10] (thrust axis [11]) of the candidate and the sphericity axis (thrust axis) of the rest of the event. The distribution of $\cos\theta_S(\theta_T)$ should be flat for B mesons and strongly peaked at ± 1.0 for continuum background. We require $|\cos\theta_S| < 0.8$ when there is a ρ or K^* meson in the final state, and $|\cos\theta_T| < 0.8$ when there is a ω meson in the final state. We also form a Fisher discriminant ($\mathcal{F}$) with event shape observables [12].

We then perform unbinned maximum-likelihood fits where the likelihood of an event is parameterized by the sum of probabilities for all relevant signal and background hypotheses, with relative weights determined by maximizing the likelihood function ($\mathcal{L}$). The probability of a particular hypothesis is calculated as a product of the probability density functions (PDFs) for each of the input observables. The observables used in the fit are ΔE, M_B, $\mathcal{F}$, $\mathcal{H}$ and the invariant mass of the resonance candidate. For final states with the same vector meson but different charged light mesons (pion or kaon), we also use the dE/dx measurement of the high-momentum track and fit for both modes simultaneously. Similarly, dE/dx measurements of the vector meson decay daughters are used in the simultaneous fit for $\bar{B}^0 \to \pi^0\rho^0$ and $\pi^0 K^{*0}$. For each decay mode investigated, the signal PDFs are determined with fits to GEANT-based simulation [13] samples. The parameters of the continuum background PDFs are determined with similar fits to simulated continuum samples as well as continuum data. Simulated continuum distributions are in excellent agreement with the data taken below the $B\overline{B}$ threshold. Correlations between observables used in the fits are investigated and their effect is found to be negligible.

In all cases, the fit includes hypotheses for signal decay modes and the dominant continuum background. Using the PDFs formed by the above observables, signal and continuum background can be well separated. For a few channels where the selected sample contains contributions from other B decays, we also include hypotheses for background from other B decay modes. These background decay modes can also be separated efficiently from the signal decay modes. We select a sample that contains both $B^- \to \pi^- \rho^0$, $K^- \rho^0$ and some contamination from $B^- \to \pi^- \bar{K}^{*0}$. We then fit simultaneously for $B^- \to \pi^- \rho^0$, $K^- \rho^0$ with and without a $B^- \to \pi^- \bar{K}^{*0}$ contribution. Similarly, we select a sample that contains both $B^- \to \pi^- \bar{K}^{*0}$, $K^- \bar{K}^{*0}$ with some contamination from $B^- \to \pi^- \rho^0$, $K^- \rho^0$. Then we perform a simultaneous fit for $B^- \to \pi^- \bar{K}^{*0}$, $K^- \bar{K}^{*0}$ with or without the $B^- \to \pi^- \rho^0$, $K^- \rho^0$ contributions. In both cases the fits with and without the background modes are consistent with each other. For each of the combinations $\bar{B}^0 \to \pi^0 \rho^0$, $\pi^0 K^{*0}$, $\bar{B}^0 \to \pi^\pm \rho^\mp$, $K^\pm \rho^\mp$, and $B^- \to \pi^- \omega$, $K^- \omega$, contributions from other B decays are negligible and we select a common sample to fit for both modes. Finally individual samples are selected and fit for the $B^- \to \pi^0 \rho^-$, $B^- \to \pi^0 K^{*-}$, $\bar{B}^0 \to \pi^0 \omega$ and $\bar{B}^0 \to K^0_S \omega$ searches.

The contributions of $b \to c$ and other B decays are small in the selected samples of final states containing three tracks or two tracks and a π^0, and their effects on the signal yields are negligible, except in the samples of $B^- \to \pi^- \rho^0$, $K^- \rho^0$ and $B^- \to \pi^- \bar{K}^{*0}$, $K^- \bar{K}^{*0}$. Events from $B^- \to D^0 \pi^-$ where $D^0 \to K^\pm \pi^\mp, \pi^+ \pi^-$ can enter into these samples and mimic our signal. We therefore impose a 30 MeV ($\sim 4\sigma$) wide $D^0 \to \pi^+ \pi^-, K^\pm \pi^\mp$ invariant mass veto in all the charged track pair combinations. We have also studied background from $B^- \to K^- \eta'$, with $\eta' \to \rho^0 \gamma$ [14,9]. This background has exactly the same final state particles as $B^- \to K^- \rho^0$ with an extra photon. Approximately 3% of this background can pass the selection for the $B^- \to \pi^- \rho^0$, $K^- \rho^0$ sample, therefore we include a component in the fit to describe this contribution. For $B^- \to \pi^0 \rho^-$ and $B^- \to \pi^0 K^{*-}$ modes, due to the limited ΔE resolution for the final state with two neutral pions, the selected sample may contain background from other B processes such as $B \to \pi a_1$, $\rho \rho$.

Table I shows the results of these measurements. The one standard deviation statistical error on the yield is determined by finding the ranges for which the quantity $\chi^2 = -2 \ln \mathcal{L}$ changes by one unit. We observe significant yields for the decays $B^- \to \pi^- \rho^0$, $\bar{B}^0 \to \pi^\pm \rho^\mp$, $B^- \to \pi^- \omega$ and $B^- \to \pi^0 \rho^-$. To verify that the yields we observe in B meson decays to three-pion final states are indeed due to $\pi\rho$ decays, we repeat the standard fit allowing for an additional three-pion "non-resonant" contribution. The PDFs for this contribution are identical to the ones used for $B \to \pi\rho$ signals except that we use PDFs that are constants in the ρ mass and $\mathcal{H}$. We find that this has no effect on the yield and the significance for $B^- \to \pi^- \rho^0$ and $\bar{B}^0 \to \pi^\pm \rho^\mp$ signals. Possible contributions from all other B processes, including higher mass pseudoscalar-vector decays, were also investigated for these channels and found to be negligible. However, the signal yield for $B^- \to \pi^0 \rho^-$ drops from $23.7^{+8.4}_{-7.4}$ with a significance of 5.1σ to $8.0^{+9.1}_{-7.9}$ events with a significance of only 1σ. We can not rule out the possibility that a significant fraction of the observed yield in $\pi^0 \rho^-$ comes from poorly measured processes such as non-resonant $\pi^- \pi^0 \pi^0$, πa_1 and $\rho\rho$ processes [9]. Therefore we calculate a conservative upper limit on the branching fraction assuming that the observed yield is due to $B^- \to \pi^0 \rho^-$ decays only.

Fig. 1 shows the likelihood contours from fits to $B^- \to \pi^- \rho^0$, $K^- \rho^0$, $\bar{B}^0 \to \pi^\pm \rho^\mp$, $K^\pm \rho^\mp$ and $B^- \to \pi^- \omega$, $K^- \omega$. The resulting branching fractions are given in Table I. Fig. 2 shows the M_B and ΔE distributions after further requirements are made on event probability to reduce background. For the remaining processes in Table I we do not consider the signal yields to be significant, and therefore set 90% C. L. upper limits for their branching fractions. Note that for the $B^- \to K^- \omega$ decay mode the additional CLEO II.V data and the re-analysis of CLEO II data no longer support its previously reported observation [6]. However, the combined branching fraction $\mathcal{B}(B^- \to h^- \omega)$

TABLE I. Measurement results. Displayed are the decay mode, event yield from the fit, total efficiency including secondary branching fraction ϵ, statistical significance (σ), branching fraction from the fit $\mathcal{B}_{fit}$ (in units of 10^{-6}), the measured branching fraction ($\mathcal{B}$) or 90% confidence level upper limit (in units of 10^{-6}) and theoretical prediction [3] (in units of 10^{-6}). For the branching fraction measurement, the first error is statistical and the second systematic. We assume equal branching fractions for $\Upsilon(4S) \to B^0\bar{B}^0$ and B^+B^-.

Decay mode	Yield	ϵ(%)	Signif.	$\mathcal{B}_{fit}$	$\mathcal{B}$ or 90% $\mathcal{B}$ UL	Theory
$B^- \to \pi^-\rho^0$	$29.8^{+9.3}_{-9.6}$	30	5.4	$10.4^{+3.3}_{-3.4} \pm 2.1$	$10.4^{+3.3}_{-3.4} \pm 2.1$	$0.4 - 13.0$
$B^- \to K^-\rho^0$	$22.4^{+10.7}_{-9.1}$	28	3.7	$8.4^{+4.0}_{-3.4} \pm 1.8$	< 17	$0.0 - 6.1$
$B^- \to \pi^-\bar{K}^{*0}$	$13.4^{+6.2}_{-5.2}$	18	3.6	$7.6^{+3.5}_{-3.0} \pm 1.6$	< 16	$3.4 - 13.0$
$B^- \to K^-\bar{K}^{*0}$	$0.0^{+2.2}_{-0.0}$	17	0.0	$0.0^{+1.3+0.6}_{-0.0-0.0}$	< 5.3	$0.2 - 1.0$
$\bar{B}^0 \to \pi^\pm\rho^\mp$	$31.0^{+9.4}_{-8.3}$	12	5.6	$27.6^{+8.4}_{-7.4} \pm 4.2$	$27.6^{+8.4}_{-7.4} \pm 4.2$	$12 - 93$
$\bar{B}^0 \to K^\pm\rho^\mp$	$16.4^{+7.8}_{-6.6}$	11	3.5	$16.0^{+7.6}_{-6.4} \pm 2.8$	< 32	$0.0 - 12.0$
$\bar{B}^0 \to \pi^0\rho^0$	$5.4^{+6.5}_{-4.8}$	34	1.2	$1.6^{+2.0}_{-1.4} \pm 0.8$	< 5.5	$0.0 - 2.5$
$\bar{B}^0 \to \pi^0\bar{K}^{*0}$	$0.0^{+3.0}_{-0.0}$	25	0.0	$0.0^{+1.3+0.5}_{-0.0-0.0}$	< 3.6	$0.7 - 6.1$
$B^- \to \pi^0\rho^-$	$23.7^{+8.4}_{-7.4}$	10	5.1	See text	< 43	$3.0 - 27.0$
$B^- \to \pi^0 K^{*-}$	$2.6^{+4.2}_{-2.6}$	4	1.0	$7.1^{+11.4}_{-7.1} \pm 1.0$	< 31	$0.5 - 24.0$
$B^- \to \pi^-\omega$	$28.5^{+8.2}_{-7.3}$	26	6.2	$11.3^{+3.3}_{-2.9} \pm 1.4$	$11.3^{+3.3}_{-2.9} \pm 1.4$	$0.6 - 24.0$
$B^- \to K^-\omega$	$7.9^{+6.0}_{-4.7}$	26	2.1	$3.2^{+2.4}_{-1.9} \pm 0.8$	< 7.9	$0.2 - 14.0$
$\bar{B}^0 \to \pi^0\omega$	$1.5^{+3.5}_{-1.5}$	19	0.6	$0.8^{+1.9+1.0}_{-0.8-0.8}$	< 5.5	$0.0 - 12.0$
$\bar{B}^0 \to \bar{K}^0\omega$	$7.0^{+3.8}_{-2.9}$	7	3.9	$10.0^{+5.4}_{-4.2} \pm 1.4$	< 21	$0.0 - 17.0$

$= (14.3^{+3.6}_{-3.2} \pm 2.0) \times 10^{-6}$ (where $h = K$ or π) is still consistent with the previous result.

Systematic errors are separated into two categories. The first consists of systematic errors in the PDFs, which are determined by varying the PDF parameters within their uncertainty. The second consists of systematic errors associated with event selection and efficiency factors. These are determined with studies of independent data samples. For branching fraction central values, the systematic error is the quadrature sum of the two components. For upper limits, the likelihood function is integrated to find the yield value that corresponds to 90% of the total area. The PDF systematic errors are taken into account in this procedure. The selection efficiency is then reduced by one standard deviation when calculating the final upper limit. As a goodness-of-fit check we compare $-2\ln\mathcal{L}$ at the minimum for our fits with expectations from fits to Monte Carlo experiments, and find them to be consistent in all cases.

In summary, we have made first observation of the decays $B^- \to \pi^-\rho^0$, $\bar{B}^0 \to \pi^\pm\rho^\mp$ and $B^- \to \pi^-\omega$. All of these $\Delta S = 0$ decay modes are expected to be dominated by hadronic $b \to u$ transitions. We see no significant yields in any of the $\Delta S = 1$ transitions. This is in contrast to the corresponding charmless hadronic B decays to two pseudo-scalar mesons ($B \to PP$) $B \to K\pi$, $\pi\pi$, where $\Delta S = 1$ transitions clearly dominate [15]. It indicates that gluonic penguin decays play less of a role in $B \to PV$ decays than in $B \to PP$ decays. This is consistent with theoretical predictions [3] that uses factorization which predicts destructive (constructive) interference between penguin operators of opposite chirality for $B \to K\rho$ ($B \to K\pi$), leading to a rather small (large) penguin contribution in these decays.

We gratefully acknowledge the effort of the CESR staff in providing us with excellent luminosity and running conditions. This work was supported by the National Science Foundation, the U.S. Department of Energy, the Research Corporation, the Natural Sciences and Engineering Research Council of Canada, the A.P. Sloan Foundation, the Swiss National Science Foundation, the Texas Advanced Research Program, and the Alexander von Humboldt Stiftung.

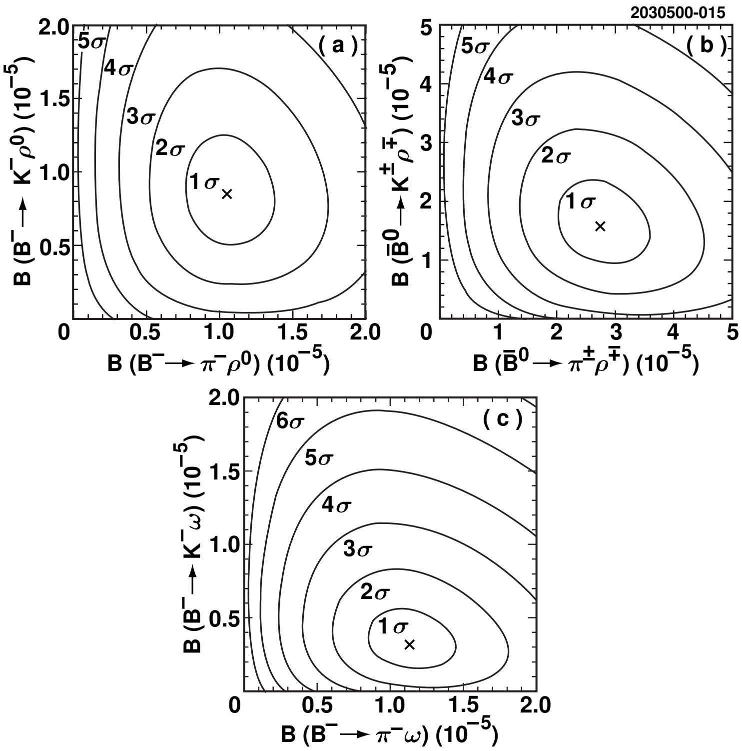

FIG. 1. Likelihood contours at n standard deviations (σ) of branching fractions for $B^- \to \pi^-\rho^0$, $K^-\rho^0$ (a), $\bar{B}^0 \to \pi^\pm\rho^\mp$, $K^\pm\rho^\mp$ (b) and $B^- \to \pi^-\omega$, $K^-\omega$ (c).

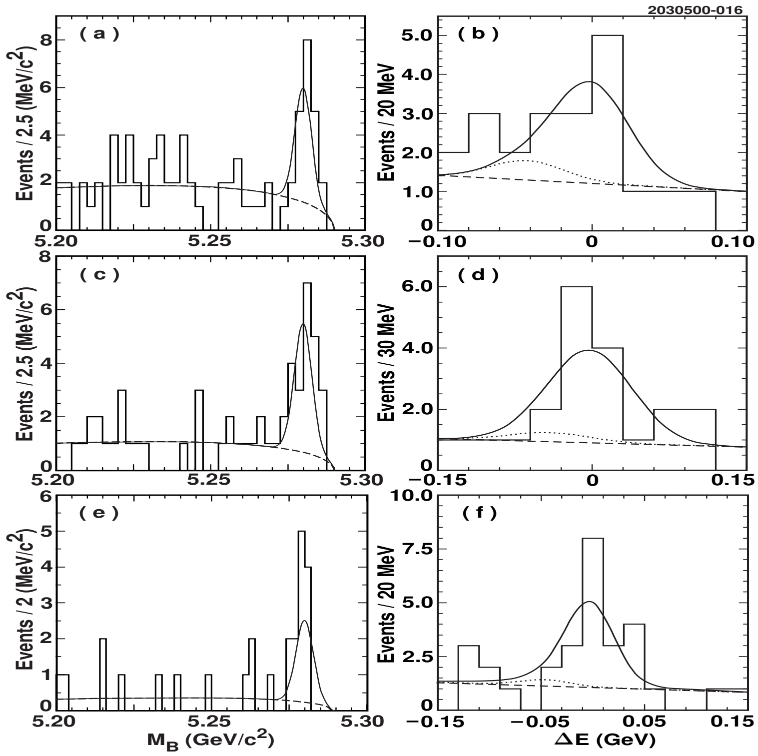

FIG. 2. Projection plots in M_B and ΔE for $B^- \rightarrow \pi^- \rho^0$ (a,b), $\bar{B}^0 \rightarrow \pi^\pm \rho^\mp$ (c,d) and $B^- \rightarrow \pi^- \omega$ (e,f). The histograms show the data while the solid lines represent the overall fit to the data scaled to account for the extra requirement on event probability applied to make the projection. The dashed lines represent the continuum and the dotted lines on top of the continuum represent the other B components ($B^- \rightarrow K^- \rho^0$, $\bar{B}^0 \rightarrow K^\pm \rho^\mp$ and $B^- \rightarrow K^- \omega$) in the simultaneous fits.

REFERENCES

[1] M. Kobayashi and T. Maskawa, Prog. Theor. Phys. **49**, 652 (1973).

[2] A. E. Snyder and H. R. Quinn, Phys. Rev. D **48**, 2139 (1993).

[3] For a review, see K. Lingel, T. Skwarnicki, J. G. Smith, Ann. Rev. Nucl. Part. Sci. **48** 253 (1998); Y-H Chen, H-Y Cheng, B. Tseng and K-C Yang, Phys. Rev. D **60** (1999) 094014.

[4] M. Neubert and J. Rosner, Phys. Lett. **B 441**, 403 (1998); N.G. Deshpande *et al.*, Phys. Rev. Lett. **82**, 2240 (1999); X.-G. He, W.-S. Hou, and K.-C. Yang, hep-ph/9902256; W.-S. Hou, J. G. Smith and F. Würthwein, hep-ph/9910014.

[5] F. Parodi, P. Roudeau, and A. Stocchi, hep-ex/9903063; S. Mele, Phys. Rev. D **59**, 113011 (1999).

[6] CLEO Collaboration, T. Bergfeld *et al.*, Phys. Rev. Lett. **81**, 272 (1998).

[7] CLEO Collaboration, Y. Kubota *et al.*, Nucl. Instrum. Methods A **320**, 66 (1992).

[8] T. Hill, Nucl. Instrum. Methods A **418**, 32 (1998).

[9] Particle Data Group, R.M. Barnett *et al.*, Phys. Rev. D **54**, 1 (1996).

[10] S. L. Wu, Phys. Rep. C **107**, 59 (1984).

[11] E. Farhi, Phys. Rev. Lett. **39**, 1587 (1977).

[12] CLEO Collaboration, D.M. Asner *et al.*, Phys. Rev. D **53**, 1039 (1996).

[13] R. Brun *et al.*, `GEANT 3.15`, CERN DD/EE/84-1.

[14] CLEO Collaboration, S. J. Richichi *et al.*, hep-ex/9912059, CLNS 99/1649, CLEO 99-16, submitted to Phys. Rev. Lett.

[15] CLEO Collaboration, D. Cronin-Hennessy *et al.*, hep-ex/0001010, CLNS 99/1650, CLEO 99-18, submitted to Phys. Rev. Lett.